Graphical Abstract:

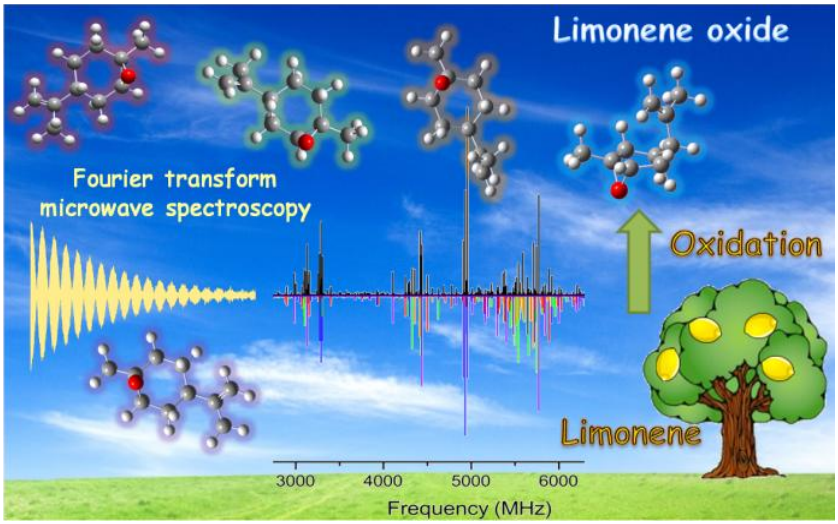

CONFORMATIONAL FLEXIBILITY OF LIMONENE OXIDE STUDIED BY MICROWAVE SPECTROSCOPY†

Donatella Loru‡[1], María Mar Quesada-Moreno‡[2,3], Juan Ramón Avilés-Moreno[3], Natasha Jarman[1], Thérèse R. Huet[3], Juan Jesús López-González[2,*] and M. Eugenia Sanz[1,*]

[1] Department of Chemistry, King's College London, London, United Kingdom.

[2] University of Jaen, Department of Physical and Analytical Chemistry, Campus Las Lagunillas, E-23071 Jaen, Spain

[3] PhLAM, UMR8523 CNRS – Université Lille 1, Bâtiment P5, F – 59655 Villeneuve d'Ascq Cedex, France

† Electronic supplementary information (ESI) available. TABLES S1-S12: Calculated spectroscopic constants of the twelve conformers of limonene oxide; TABLE S13: Calculated relative energies of the *t*TS1, *t*TS2, *t*TS3, *c*TS1, *c*TS2 and *c*TS3 transition states for the equatorial and axial conformations; TABLES S14-S18: Transitions measured for I, II, III, IV and V conformers; FIGURE S1: Potential energy surface of the lowest-energy equatorial conformation of limonene oxide along the two methyl groups torsion coordinates; FIGURE S2: Calculated methyl internal torsion barriers for the observed axial conformer of limonene oxide; FIGURE S3: Weighted VCD spectrum taking into account the five most stable equatorial conformers and the lowest-energy axial conformer. See DOI: 10.1039/....

‡ These two authors contributed equally to this paper, and share first authorship.

Corresponding author's name, mailing address and e-mail address:
Prof. Juan Jesús López González
University of Jaen, Department of Physical and Analytical Chemistry, Campus Las Lagunillas, E-23071 Jaen, Spain
E-mail : jjlopez@ujaen.es

Dr. M. Eugenia Sanz
Department of Chemistry, King's College London, London SE1 1 DB, United Kingdom
E-mail : maria.sanz@kcl.ac.uk

ABSTRACT

Monoterpenoids are biogenic volatile organic compounds (BVOCs) that play a major role in atmospheric chemistry, participating in the formation of aerosols. In this work, the monoterpenoid *R*-(+)-limonene oxide ($C_{10}H_{16}O$) has been characterized in the gas phase by Fourier transform microwave spectroscopy in a supersonic jet. Five conformers of limonene oxide, four equatorial and one axial considering the configuration of the isopropenyl group, have been unambiguously identified from the analysis of the rotational spectrum. The observed conformers include *cis* and *trans* forms, and are stabilised by a subtle balance of hydrogen bonds, dispersive interactions and steric effects. Estimated conformational relative abundances surprisingly reveal that the axial conformer has an abundance similar to some equatorial conformers. In addition, the potential energy surface was extensively explored using density functional theory and *ab initio* methods.

1. Introduction

Terpenoids, formed by combining and modifying five carbon isoprene units and adding substituents to them, are one of the main groups of secondary metabolites in nature, with nearly 23000 being characterised [1,2]. They show a variety of chemical and biological activities [3], such as antitumor [4], antibacterial [5], antioxidant [6] and antifungal properties [7].

Monoterpenoids, with 10 carbon atoms (derived from the combination of two isoprene units), are the principal volatiles released by different plants and coniferous forests, and are emitted in large quantities. Most monoterpenoids are unsaturated hydrocarbons and react very fast with atmospheric constituents, especially with ozone and hydroxyl radicals, forming oxidation products that can produce secondary organic aerosols (SOAs) [8-12]. Monoterpenoids are thus biogenic volatile organic compounds (BVOCs) that play an important role in atmospheric chemistry as they are linked with climate change in a variety of ways [8].

In order to clarify the role of terpenoid chemistry in the atmosphere, a major challenge is the identification and quantification of the semi-volatile compounds formed by oxidation processes [10,13]. To this end, techniques such as two dimensional heteronuclear NMR spectroscopy [14], Fourier transform infrared spectroscopy (FTIR) [15], proton transfer reaction mass spectrometry (PTR-MS) [16], high-performance liquid chromatography (HPLC) [15] and gas chromatography coupled with mass spectrometric detection [17,18] have been widely applied. Recently, high-resolution microwave spectroscopy has also been employed to study the structure in gas phase of several terpenoids, namely, perillaldehyde [1], carvone [19,20], limonene [19], carvacrole and thymol [21], menthone and menthol [2], 4-carvomenthenol [22], camphor [23], and fenchone [24] among others.

Limonene oxide (4-isopropenyl-1-methyl-7-oxabicyclo[4.1.0]heptane, Fig. 1) is an atmospheric pollutant produced by oxidation of other terpenes, mostly by degradation of limonene and α-pinene [25]. The molecular structure and VCD spectrum of limonene oxide were investigated by S. Abbate *et al.* in the near infrared and visible range [26]. J. R. Avilés-Moreno *et al.* studied the structure of this molecule theoretically and analysed the experimental IR, Raman and Vibrational Circular Dichroism (VCD) spectra in liquid phase with the help of quantum chemical calculations at the B3LYP/cc-pVDZ level of theory [27], finding that the experimental data could be explained by considering a mixture of equatorial conformers.

In the present work we investigate limonene oxide in the gas phase for the first time, uniquely characterising its conformations by Fourier-transform microwave (FTMW) spectroscopy in supersonic jets and carrying out higher level quantum chemical calculations. Five different conformers of limonene oxide have been detected, and their molecular parameters determined, from the analysis of its rotational spectrum. The potential energy surface (PES) of limonene oxide has been explored with density functional theory and *ab initio* methods using several basis sets. Comparison of the experimental rotational constants with those calculated ab initio led to the conclusive identification of the species observed in the rotational spectrum as four equatorial and one axial conformers. Attractive interactions such as hydrogen bonds and dispersion forces, together with steric effects, have been found to be relevant in determining conformer structures. In addition, possible conformational relaxation processes in the supersonic jet have been investigated with MP2 calculations. The gas phase results reported here are compared with those obtained for the liquid phase. The present study provides definite information on the conformational landscape of a relevant monoterpenoid of environmental and atmospheric interest, and on the factors that govern its conformational preferences.

2. Methods

2.1. Experimental

The microwave spectrum of limonene oxide was recorded in the frequency range 4–20 GHz using an impulse Fabry-Pérot molecular beam Fourier transform microwave FP-FTMW spectrometer [27-30] available in Lille, and in the frequency range 2-8 GHz using a chirp FTMW (CP-FTMW) spectrometer at King's College London [24]. *R*-(+)-limonene oxide was purchased from Sigma–Aldrich as a mixture of *cis* and *trans* isomers (97% purity) and used without further purification. In both experiments, a few droplets of neat liquid were placed in a bespoke heating nozzle and heated at temperatures of 343-353 K to obtain optimal signals, as limonene oxide has a low vapour pressure at room temperature.

In the FP-FTMW experiment, neon flowed through the heated nozzle at a stagnation pressure of 2 bar. The gas mixture was then introduced into the vacuum tank containing the Fabry-Perot cavity, by means of the pulsed nozzle at a rate of 1.5 Hz, to create a supersonic beam with an estimated T_{rot} = 0.5-1 K. The molecules were polarized with 2 μs pulses of tunable microwave radiation and the free-induction decay occurring at each resonance frequency was detected and processed. As the nozzle is located in the centre of the fixed mirror of the Fabry-Perot cavity, the supersonic expansion is coaxial to the optical axis leading to a characteristic Doppler doubling in the spectrum [31]. The experimental retained frequency of the lines is the average frequency of the two Doppler components (10 kHz full width at half-maximum, FWHM) after Fourier transformation 65536 data points sampled at 120 MHz leading to a frequency grid of 1.84 kHz.

In the CP-FTMW experiment, limonene oxide was seeded in neon at stagnation pressures of 5 bar. Molecular pulses of 1100 μs were found optimal to form the supersonic jet in our vacuum chamber. Limonene oxide molecules were polarised with chirps of 4 μs

duration spanning the 2-8 GHz frequency range. Molecular relaxation signals were collected in the time domain for 15 μs using a digital oscilloscope. A fast Fourier-transform algorithm with a Kaiser-Bessel window was used to convert the transient record into the frequency domain. In our setup the microwave radiation propagates perpendicular to the supersonic jet, which results in a short transit time of the molecules through the MW field region, and with the settings above this yields lines with FWHM ~ 110 kHz.

2.2. Computational

Theoretical calculations were carried out to explore the conformational landscape of limonene oxide and optimise the structures of its lower-energy conformers, predicting their molecular properties and aiding conformational identification. All calculations were performed using the Gaussian 09 software package [32].

As explained in ref. [27], there are 12 conformational minima in the potential energy surface (PES) of limonene oxide, corresponding to the combinations of six possible conformations of the isopropenyl group (equatorial and axial, each at three dihedral angles $\angle C_8C_7C_4C_5$ around 0° (**C**), +120° (**A**) and -120° (**a**), with a *cis* or *trans* configuration of the epoxide ring with respect to the isopropenyl group (see Fig. 2). The calculations performed in ref. [27] using B3LYP in combination with the 6-31G** and the cc-pVDZ basis sets have been significantly extended here to include the M06-2X functional and *ab initio* (MP2) methods [33-36]. The structures of the 12 conformational minima were optimised at the B3LYP/6-311++G(d,p), B3LYP/6-311++G(2df,p), B3LYP-D3/6-311G++(d,p) Grimme's D3 dispersion [37], M062X/6-311++G(d,p), M062X/6-311++G(2df,p), MP2/6-311++G(d,p) and MP2/aug-cc-pVTZ levels of theory. The relative energies of the conformers were determined using the above methods, and also the G3 and G4 methodologies (see Table 1). There are considerable changes in going from B3LYP (with and without Grimme's D3 dispersion) to

M06-2X and MP2 methods; specifically, the latter methods predict all axial conformers to have considerably lower energies, which results in a different energy ordering with one of the axial forms now predicted to be the global minimum. The rotational constants and dipole moment components for all conformers predicted by each method are collected in Tables S1-S12 of the Supplementary Information. Table 2 displays the MP2/6-311++G(d,p) values.

The PES of limonene oxide has been also explored along the isopropenyl group torsional coordinate for axial and equatorial conformers by scanning the dihedral angle $\angle C_8C_7C_4C_5$ (see Fig. 1) in steps of 5° at the MP2/6-311++G(d,p) level of theory (see Fig. 4). This confirmed the energy ordering of the conformers, and allowed us to investigate conformational interconversion and identify transition states. Higher energy conformers can relax to their lower energy forms by collisions with the carrier gas in the initial stages of the supersonic expansion, if barriers for interconversion are sufficiently low, around 1000 cm^{-1} (*ca.* 12 kJ/mol) or lower, for molecular systems with several degrees of freedom [38-40]. Considering this, conformers **eq-trans-C**, **eq-cis-C**, **ax-trans-a** and **ax-cis-A,** predicted to have very low interconversion barriers to conformers **eq-trans-A, eq-cis-A**, **ax-trans-A** and **ax-cis-a**, respectively, are extremely likely to relax in the supersonic jet. The structures of the transition states between all forms have been optimised at different levels of theory. Their relative energies are given in Table S13 of the Supplementary Information.

The torsional barriers of the two methyl groups of limonene oxide have also been explored by carrying out scans along the $\angle HC_9C_7C_4$ and $\angle HC_{10}C_1C_6$ dihedral angles (see Fig. 1 for atom labelling) at B3LYP/6-311++G(2df,p), M062X/6-311++G(2df,p) and MP2/6-311++G(d,p) levels of theory. Barriers of 750 (B3LYP), 680 (M062X) and 890 (MP2) cm^{-1} for the $\angle HC_{10}C_1C_6$ dihedral angle and 500 cm^{-1} at the three levels of theory for the $\angle HC_9C_7C_4$ dihedral angle were calculated for the lowest-energy equatorial conformer (see Fig. S1 in the Supplementary Information). Methyl torsion barriers of *ca.* 900 cm^{-1} and 650

cm^{-1} were calculated along the $\angle HC_{10}C_1C_2$ and $\angle HC_9C_7C_4$ dihedral angles, respectively, using MP2/6-311++G(d,p) for the lowest-energy axial form (see Fig. S2 in the Supplementary Information.

3. Rotational Spectrum

The rotational spectrum of limonene oxide was observed and assigned using both FP-FTMW and CP-FTMW spectrometers in Lille and London, respectively. The broadband rotational spectrum of limonene oxide in the 2-8 GHz frequency range is displayed in Fig. 3. On first inspection, the spectrum presents a high density of lines which seems to indicate the presence of several conformations. All conformers of limonene oxide are expected to be asymmetric tops close to the prolate limit, and most have sizable values of the μ_b dipole moment (see Table 2). Therefore first searches were directed to find the series of R-branch *b*-type transitions $J_{1,J-1} \leftarrow J_{0,J}$ separated by approximately 2C. Four species were initially found in the spectrum. First fits including *b*-type transitions allowed us to determine preliminary rotational constants and to predict more transitions that were later measured and incorporated in the fits, confirming original assignments. All transitions were fitted according to a standard Watson-type Hamiltonian (S-reduction and I^r representation) [41] using the non-linear least-squares fit program developed by Pickett [42]. Transitions measured in Lille were accounted for at uncertainties of 2 kHz and those measured in London were weighted at uncertainties of 10 kHz. The determined rotational and quartic centrifugal distortion constants are listed in the first four columns of Table 3. After removing the transitions assigned to these four species from the 2-8 GHz spectrum, many lines still remained. A series of lines showing the typical pattern of R-branch, *a*-type transitions belonging to a prolate asymmetric top were identified. Following the same procedure as outlined above, more transitions were measured and a final

fit yielded the spectroscopic constants in the fifth column of Table 3. All measured transitions are collected in Tables S14-S18 in the Supplementary Information.

Assignment of the species observed to individual conformers is achieved by comparing the experimental molecular properties, in this case rotational constants and dipole moment components, with those predicted theoretically. Although all conformers of limonene oxide are predicted to be asymmetric tops close to the prolate limit, the significant differences in mass distribution between axial and equatorial conformers are clearly reflected in the values of the rotational constants in Table 2. Considering the values of *A*, *B* and *C*, it is evident that the species **I-IV** in the first four columns of Table 3 are equatorial conformers while that in the fifth column is an axial form. By comparing the theoretical and experimental values of the rotational constants, and using the values of the inertial defect, it is possible to assign unambiguously the observed conformers. Species **I** corresponds to conformer **eq-cis-a**, species **II** is **eq-trans-a**, species **III** is **eq-trans-A** and species **IV** is **eq-cis-A**. The axial form, species **V** is conformer **ax-trans-C**.

The assignment is further confirmed by considering the theoretical values of the dipole moment components along the *a*, *b*, and *c* inertial axes for the different conformers and comparing them with the relative intensities of *a*-, *b*- and *c*-type transitions, which are proportional to the corresponding dipole moment component or to its square in the polarisation optimized FP-FTMW or in the linear fast passage CP-FTMW experiment, respectively. For all conformers, the relative intensities observed for the *a*-, *b*- and *c*-type transitions (see Table 3) are in excellent agreement with the theoretical values of μ_a, μ_b, and μ_c (Table 2). Furthermore, to optimise molecular polarisation by the use of a $\pi/2$ pulse in the FP-FTMW experiment, the amplitude of the electric field had to be adjusted for each line type proportional to the value of the components of the permanent dipole moment. For **eq-trans-A** and **eq-trans-a** conformers, the excitation powers needed for the *a*-type, *b*-type, and *c*-type

transitions indicate that the electric dipole moment components satisfy the inequality $\mu_c > \mu_b > \mu_a$. For the **eq-cis-a** conformer, the excitation powers needed for optimum polarisation, indicate that $\mu_c \approx \mu_b > \mu_a$.

No splittings of the measured transitions due to methyl group internal rotation were observed, in agreement with expectations from the calculated barriers. Splittings between A and E symmetry transitions components were calculated to be ~1 kHz for the observed axial and equatorial conformers with the lowest predicted methyl torsion barriers using the program XIAM [43], and therefore not resolvable in our experiments. Following removal of all measured transitions, a large number of lines still remain in the 2-8 GHz. Despite several attempts, it has not been possible to assign further conformers of limonene oxide.

The abundances of the conformers of limonene oxide can be estimated from relative intensity measurements of selected transitions. Referring to the intensity dependence given above, the estimated abundances from comparison of *b*-and *c*-type transitions, where available, in the CP-FTMW experiment are **eq-trans-a** > **eq-cis-A** > **eq-trans-A** ≈ **eq-cis-a** ≈ **ax-trans-C**. These abundances are consistent with those from the FP-FTMW experiment, estimated as **eq-trans-a > eq-trans-A** ≈ **eq-cis-a**. Ab initio abundances, from the MP2 values of the Gibbs free energies calculated at 353 K (see Table 2), predict conformer **eq-trans-A** as the most abundant, with very similar abundances for all equatorial conformers and conformer **ax-trans-C,** while the rest of the axial conformers abundances are much lower (the higher is 4%).

4. Discussion

There are several conformers of limonene oxide that have not been observed in the rotational spectrum. In the case of conformers **eq-trans-C** and **eq-cis-C**, this can be explained by the very low barriers predicted for the interconversion to conformers **eq-trans-A** and **eq-**

cis-A, respectively (see Fig. 4a), and therefore they are very likely to relax to lower-energy forms by collisions in the supersonic expansion. Similarly low energy barriers are predicted for the conversion of **ax-cis-A** and **ax-trans-a** to **ax-cis-a** and **ax-trans-A**, respectively (see Fig. 4b). Given their relative energies, the remaining axial conformers (**ax-cis-C**, **ax-cis-a** and **ax-trans-A**) have probably not been observed because they are not sufficiently populated in our experiments. Similar observations regarding relaxation of higher energy conformers to lower-energy ones have been reported for the related terpenes perillaldehyde [1], menthol [2], carvone [19], and limonene [19].

The preferred four equatorial and one axial conformations of limonene oxide can be rationalised in terms of minimal steric effects and maximum attractive interactions. The epoxide ring of limonene oxide is highly reactive because of its strain, and it has a strong electron acceptor that can establish weak C–H···O hydrogen bonds. These hydrogen bonds can be formed by interactions of the lone electron pairs of the oxygen in the epoxide ring with one of the hydrogens of the six-membered ring, or with one of the hydrogens of the methyl or methylene groups in the isopropenyl substituent. Furthermore, there will be steric effects and dispersive interactions due to the proximity of the methyl and/or methylene groups of the isopropenyl substituent to the $–CH_2–$ in the six-membered ring.

Because the theoretical MP2/6-311++G(d,p) rotational constants are very close to the experimental ones, with differences smaller than 0.9 % for all equatorial conformers (and generally smaller than 0.4%) and 3% for the axial one, it is reasonable to assume that the MP2 predictions are close to the actual structures of the limonene oxide conformers. Specially, the C–H···O hydrogen bond lengths of limonene oxide conformers are within the range of those reported for C–H···O bonds of the simplest epoxide ring (oxirane) with methane derivatives in the gas phase [44,45]. The exception is conformer **ax-cis-A**, with a shorter hydrogen bond. Looking at the isopropenyl group, its configuration in axial *cis* conformers brings it in close

proximity to the epoxide and six-membered rings, increasing destabilising interactions between the $–CH_3$ or $–CH_2$ groups of the isopropenyl group with the $–CH_2–$ in the six-membered ring. A similar situation can be found for the **ax-trans-a** and **ax-trans-A** conformers. The **ax-trans-C** conformer, however, adopts a configuration where one of the H atoms of C_3 in the six-membered ring is at a shorter distance (2.68 Å) from the oxygen in the epoxide ring than the other axial *trans* forms, while the hydrogens in the isopropenyl group are further away from the hydrogens of the six-membered ring. This delicate balance of forces reduces the energy of the **ax-trans-C** conformer and therefore allowing its observation. The equatorial conformers present less steric effects due to the different arrangement of the isopropenyl group. All of them show similar distances (2.59 Å – 2.69 Å) between the oxygen in the epoxide ring and one H atom of C_3 or the H atom of C_4. The differences in energy for the equatorial conformers appear to be related to the interactions between the H atoms of the $–CH_3$ or $–CH_2$ groups of the isopropenyl group and the H atoms of the $–CH_2–$ in the six-membered ring, as shorter distances correspond to equatorial conformers predicted to lie at higher energies.

The structures of equatorial conformers are predicted to be closer to the experimental ones than those of axial conformers at all levels of theory used. The energy ordering of the equatorial conformers is maintained qualitatively across all methods. The axial conformers, however, are predicted to lie much higher in energy by B3LYP than with M062X or MP2 methods. The main difference between axial and equatorial conformers is the existence of long-range interactions between the isopropenyl group and the six-membered and epoxide rings in the axial conformers. B3LYP is well-known for not being a particularly effective method in considering long-range dispersive interactions while B3LYP-D3, M062X and MP2 include these effects with more success [46]. The observation of conformer **ax-trans-C**

validates the latter methods and illustrates the significant effect of dispersion forces in conformational energies.

Limonene oxide has been studied in the liquid phase by some of us using IR-Raman-VCD spectroscopy at room temperature [27]. In that work, the recorded spectra, particularly the VCD spectrum of limonene oxide, could be reproduced from theoretical data at the B3LYP/cc-pVDZ level only by including the contributions from the five equatorial conformers **eq-trans-a** (eq-t110, 34%), **eq-trans-A** (eq-t255, 16%), **eq-cis-a** (eq-c110, 15%), **eq-cis-A** (eq-c255, 12%) and **eq-cis-C** (eq-c305, 11%), considering a Boltzmann distribution at room temperature. As we had detected the **ax-trans-C** (ax-t345 conformer in the reference 27) conformer in the gas phase and M06-2X and MP2 methods and G3 methodology predicted it to be the lowest-energy conformer, we checked its presence in liquid phase by recalculating the weighted theoretical VCD spectra by adding its theoretical VCD contribution with Boltzmann populations given by the MP2 method. However, the agreement was better between the experimental VCD spectrum and the weighted VCD spectrum taking into account the five most stable equatorial conformers, *i.e.*, **eq-trans-a** (eq-t110, 43%), **eq-trans-A** (eq-t255, 13%), **eq-cis-a** (eq-c110, 18%), **eq-cis-A** (eq-c255, 10%) and **eq-cis-C** (eq-c305, 8%), than between the experimental VCD spectrum and the weighted VCD spectrum taking into account the five most stable equatorial conformers and the lowest-energy axial conformer, *i.e.*, **ax-trans-C** (ax-t345, 37%), **eq-trans-a** (27%), **eq-trans-A** (8%), **eq-cis-a** (11%), **eq-cis-A** (6%) and **eq-cis-C** (5%) conformers (see Fig. S3 in the Supplementary Information). We can notice that especially in the 1500-1400 cm^{-1} and 1150-900 cm^{-1} spectral regions, where the correspondence between experiment and theory is worse considering the theoretical VCD contribution of **ax-trans-C** conformer. Thus, the conformational landscape of limonene oxide changes with the phase. In the gas phase, the **ax-trans-C** conformer is predicted as the lowest-energy form and has a significant abundance. In the liquid phase,

conformer **ax-trans-C** is not present and the most abundant conformer is the **eq-trans-a**, which is also present in the gas phase.

5. Conclusion

A systematic and detailed conformational study, using FT-MW spectroscopy, of *R*-(+)-limonene oxide in the gas phase has been accomplished for the first time. Analysis of the experimental data aided by high-level quantum chemical calculations allowed us to characterise the conformational landscape of this relevant atmospheric species. Four equatorial and one axial conformations have been identified, referring the position of the isopropenyl group. The observed conformers include *cis* and *trans* forms.

The observation of an axial conformer with similar abundance as some equatorial conformers challenges assumptions that equatorial forms are generally more stable, and reflects the delicate balance of forces at play in limonene oxide, which include attractive interactions involving the epoxide ring, dispersive interactions involving the isoproprenyl group, and steric effects.

The behaviour of limonene oxide in the gas and liquid phases has been compared, showing how the phase affects conformational preferences.

Acknowledgements

The CaPPA project (Chemical and Physical Properties of the Atmosphere) is funded by the French National Research Agency (ANR) through the PIA (Programme d'Investissement d'Avenir) under contract ANR-10-LABX-005. MMQM thanks the University of Jaén for a predoctoral fellowship and the University of Lille 1 for a visiting fellowship through contract ANR-10-BLAN-724-5 NCPCHEM. Authors are also thankful to the *Centro de Servicios de Informática y Redes de Comunicaciones* (CSIRC), University of Granada (UGR), for

computational time and facilities. DL, NJ and MES would like to thank funding from EU FP7 (grant PCIG12-GA-2012-334525) and King's College London.

REFERENCES

1 J. R. Avilés Moreno, F. Partal Ureña, J. J. López González and T. R. Huet, *Chem. Phys. Lett.*, 2009, **473**, 17–20.

2 D. Schmitz, V. A. Shubert, T. Betz and M. Schnell, *Front. Chem.,* 2015, **3**:15.

3 K.-H. Wagner and I. Elmadfa, *Ann. Nutr. Metab.*, 2003, **47**, 95-106.

4 P. L. Crowell, S. Lin, E. Vedejs and M. N. Gould, *Cancer Chemother. Pharmacol*., 1992, **31**, 205-212.

5 D. Trombetta, F. Castelli, M. G. Sarpietro, V. Venuti, M. T. Cristani, C. Daniele, A. Saija, G. Mazzanti and G. Bisignano, *Antimicrob. Agents Chemother.*, 2005, **49**, 2474–2478.

6 G. Ruberto and M. T. Baratta, *Food. Chem.*, 2000, **69**, 167-174.

7 M. A. Numpaque, L. A. Oviedo, J. H. Gil, C. M. García and D. L. Durango, *Trop. Plant. Pathol.*, 2011, **36**, 3–13.

8 R. Matyssek, N. Clarke, P. Cudlin, T. N. Mikkelsen, J-P. Tuovinen, G. Wieser and E. Paoletti, *Climate Change, Air Pollution and Global Challenges: Understanding and Perspectives from Forest Research,* Elsevier, Oxford, UK, 2013.

9 G. Restelli and G. Angeletti, *Physico-Chemical Behaviour of Atmospheric Pollutants (1989): Air Pollution Research Reports,* Springer Science & Business Media, Luxembourg, 2012.

10 M. L. Walser, J. Park, A. L. Gomez, A. R. Russell and S. A. Nizkorodov. *J. Phys. Chem. A,* 2007, **111**, 1907–1913.

11 A. Calogirou, B. R. Larsen and D. Kotzias, *Atmos. Environ.,* 1999, **33**, 1423-1439.

12 H. Ourrad, F. Thevenet, V. Gaudion and V. Riffault, *Appl. Catal. B*, 2015, **168-169**, 183–194.

13 J. L. Fry, A. Kiendler-Scharr, A. W. Rollins, T. Brauers, S. S. Brown, H.-P. Dorn, W. P. Dube, H. Fuchs, A. Mensah, F. Rohrer, R. Tillmann, A. Wahner, P. J. Wooldridge and R. C. Cohen, *Atmos. Chem. Phys.*, 2011, **11**, 3879–3894.

14 C. S. Maksymiuk, C. Gayahtri, R. R. Gil and N. M. Donahue, *Phys. Chem. Chem. Phys.*, 2009, **11**, 7810-7818.

15 V. Librando and G. Tringali, *J. Environ. Manage.*, 2005, **75**, 275-282.

16 Y. Ishizuka, M. Tokumura, A. Mizukoshi, M. Noguchi and Y. Yanagisawa, *Int. J. Environ. Res. Public. Health*, 2010, **7**, 3853–3870.

17 S. S. Marine and J. Clemons, *J. Chromatogr. Sci.*, 2003, **41**, 31-35.

18 L. Chiappini, S. Rossignol, E. Mombelli, C. Greuillet, J. Nicolle and M. Nicolas, *SOA formation study from limonene ozonolysis in indoor environment: gas and particulate phases chemical characterization and toxicity prediction*, 10. International Conference Healthy Buildings (HB2012), 2012, Brisbane, Australia. Queensland University of Technology, pp.NC.

19 J. R. Avilés Moreno, T. R. Huet and J. J. López González, *Struct. Chem.*, 2013, **24**, 1163–1170.

20 V. A. Shubert, D. Schmitz, D. Patterson, J. M. Doyle and M. Schnell, *Angew. Chem. Int. Ed.*, 2014, **53**, 1152 –1155.

21 D. Schmitz, V. A. Shubert, B. M. Giuliano and M. Schnell, *J. Chem. Phys.*, 2014, **141**, 034304.

22 V. A. Shubert, D. Schmitz, C. Medcraft, A. Krin, D. Patterson, J. M. Doyle and M. Schnell, *J. Chem. Phys.*, 2015, **142**, 214201.

23 Z. Kisiel, O. Desyatnyk, E. Białkowska-Jaworska and L. Pszczółkowski. *Phys. Chem. Chem. Phys.*, 2003, **5**, 820–826.

24 D. Loru, M. A. Bermúdez and M. E. Sanz, *J. Chem. Phys*. **145**, 074311 (2016).

25 P. Oliveira, M. L. Rojas-Cervantes, A. M. Ramos, I. M. Fonseca, A. M. Botelho do Rego and J. Vital, *Catal. Today*, 2006, **118**, 307–314.

26 S. Abbate, G. Longhi, S. Boladjiev, D. A. Lightner, C. Bertucci and P. Salvadori, *Enantiomer*, 1998, **3**, 337–347.

27 J. R. Avilés Moreno, F. Partal Ureña and J. J. López González, *Phys. Chem. Chem. Phys.*, 2009, **11**, 2459–2467.

28 J. R. Aviles-Moreno, J. Demaison and T. R. Huet, *J. Am. Chem. Soc.*, 2006, **128**, 10467-10473.

29 M. Rey, J. R. Aviles-Moreno and T. R. Huet, *Chem. Phys. Lett.*, 2006, **430**, 121-126.

30 J. R. Aviles-Moreno, D. Petitprez and T. R. Huet, *Chem. Phys. Lett.*, 2006, **419**, 411-416.

31 J. U. Grabow, W. Stahl and H. Dreizler, *Rev. Sci. Instrum.*, 1996, **67**, 4072-4084.

32 M. J. Frisch, G. W. Trucks, H. B. Schlegel, G. E. Scuseria, M. A. Robb, J. R. Cheeseman, G. Scalmani, V. Barone, B. Mennucci, G. A. Petersson, H. Nakatsuji, M. Caricato, X. Li, H. P. Hratchian, A. F. Izmaylov, J. Bloino, G. Zheng, J. L. Sonnenberg, M. Hada, M. Ehara, K. Toyota, R. Fukuda, J. Hasegawa, M. Ishida, T. Nakajima, Y. Honda, O. Kitao, H. Nakai, T. Vreven, J. A. Montgomery, Jr., J. E. Peralta, F. Ogliaro, M. Bearpark, J. J. Heyd, E. Brothers, K. N. Kudin, V. N. Staroverov, R. Kobayashi, J. Normand, K. Raghavachari, A. Rendell, J. C. Burant, S. S. Iyengar, J. Tomasi, M. Cossi, N. Rega, J. M. Millam, M. Klene, J. E. Knox, J. B.

Cross, V. Bakken, C. Adamo, J. Jaramillo, R. Gomperts, R. E. Stratmann, O. Yazyev, A. J. Austin, R. Cammi, C. Pomelli, J. W. Ochterski, R. L. Martin, K. Morokuma, V. G. Zakrzewski, G. A. Voth, P. Salvador, J. J. Dannenberg, S. Dapprich, A. D. Daniels, Ö. Farkas, J. B. Foresman, J. V. Ortiz, J. Cioslowski and D. J. Fox, Gaussian 09, Revision B.01, Gaussian, Inc., Wallingford CT, 2010.

33 A. D. Becke, *J. Chem. Phys.*, 1993, **98**, 5648–5652.

34 C. Lee, W. Yang and R. G. Parr, *Phys. Rev. B*, 1988, **37**, 785–789.

35 Y. Zhao and D. Truhlar, *Theor. Chem. Acc.*, 2008, **120**, 215–241.

36 C. Møller and M. S. Plesset, *Phys. Rev.*, 1934, **46**, 618–622.

37 S. Grimme, J. Antony, S. Ehrlich and H. Krieg, *J. Chem. Phys.*, 2010, **132**, 154104.

38 R. S. Ruoff, T. D. Klots, T. Emilsson and H. S. Gutowsky, *J. Chem. Phys.*, 1990, **93**, 3142-3150.

39 (a) P. D. Godfrey and R. D. Brown, *J. Am. Chem. Soc.*, 1998, **120**, 10724-10732; (b) G. M. Florio, R. A. Christie, K. D. Jordan and T. S. Zwier, *J. Am. Chem. Soc.*, 2002, **124**, 10236-10247.

40 M. Goubet, R. A. Motiyenko, F. Réal, L. Margulès, T. R. Huet, P. Asselin, P. Soulard, A. Krasnicki, Z. Kisiel and E. A. Alekseev, *Phys. Chem. Chem. Phys.*, 2009, **11**, 1719-1728.

41 J. K. G. Watson, *Vibrational Spectra and Structure*, Elsevier, New York/Amsterdam, 1977.

42 H. M. Pickett, *J. Chem. Phys.*, 1972, **56**, 1715.

43 H. Hartwig and H. Dreizler, *Z. Naturforsch.*, 1996, **51a**, 923-932.

44 J. L. Alonso, S. Antolínez, S. Blanco, A. Lesarri, J. C. López and W. Caminati, *J. Am. Chem. Soc.*, 2004, **126**, 3244-3249.

45 S. Blanco, A. Lesarri, J. C. López, W. Caminati and J. L. Alonso, *ChemPhysChem*, 2004, **5**, 1779 –1782.

46 S. T. Shipman, J. L. Neill, R. D. Suenram, M. T. Muckle and B. H. Pate, *J. Phys. Chem. Lett.*, 2011, **2**, 443–448.

LIST OF FIGURES

TABLE CAPTION

TABLE 1. Relative energies of the twelve conformers of limonene oxide from several levels of theory.

TABLE 2. Theoretical spectroscopic constants and dipole moment components of the axial and equatorial conformers of limonene oxide using MP2/6-311++G(d,p) including zero-point corrections.

TABLE 3: Experimental spectroscopic constants for the five observed rotamers of limonene oxide.

FIGURES

FIGURE 1

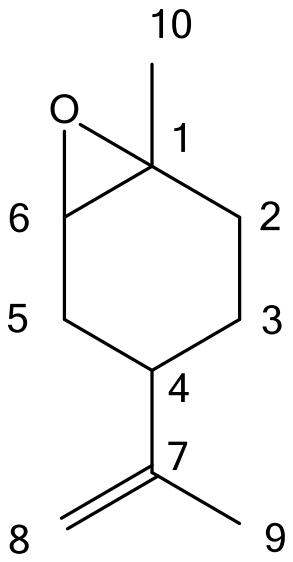

FIGURE 2

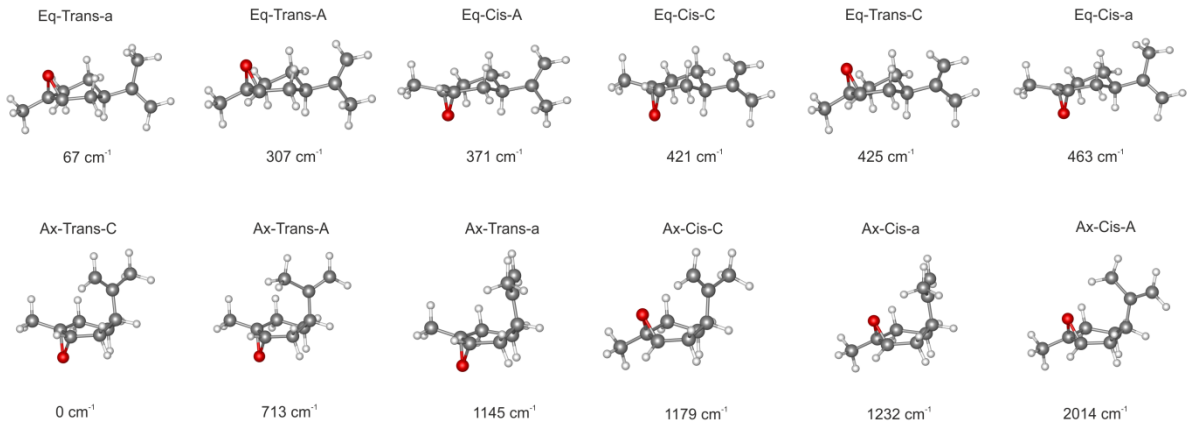
Eq-Trans-a
67 cm-1
Eq-Trans-A
307 cm-1
Eq-Cis-A
371 cm-1
Eq-Cis-C
421 cm-1
Eq-Trans-C
425 cm-1
Eq-Cis-a
463 cm-1
Ax-Trans-C
0 cm-1
Ax-Trans-A
713 cm-1
Ax-Trans-a
1145 cm-1
Ax-Cis-C
1179 cm-1
Ax-Cis-a
1232 cm-1
Ax-Cis-A
2014 cm-1

FIGURE 3

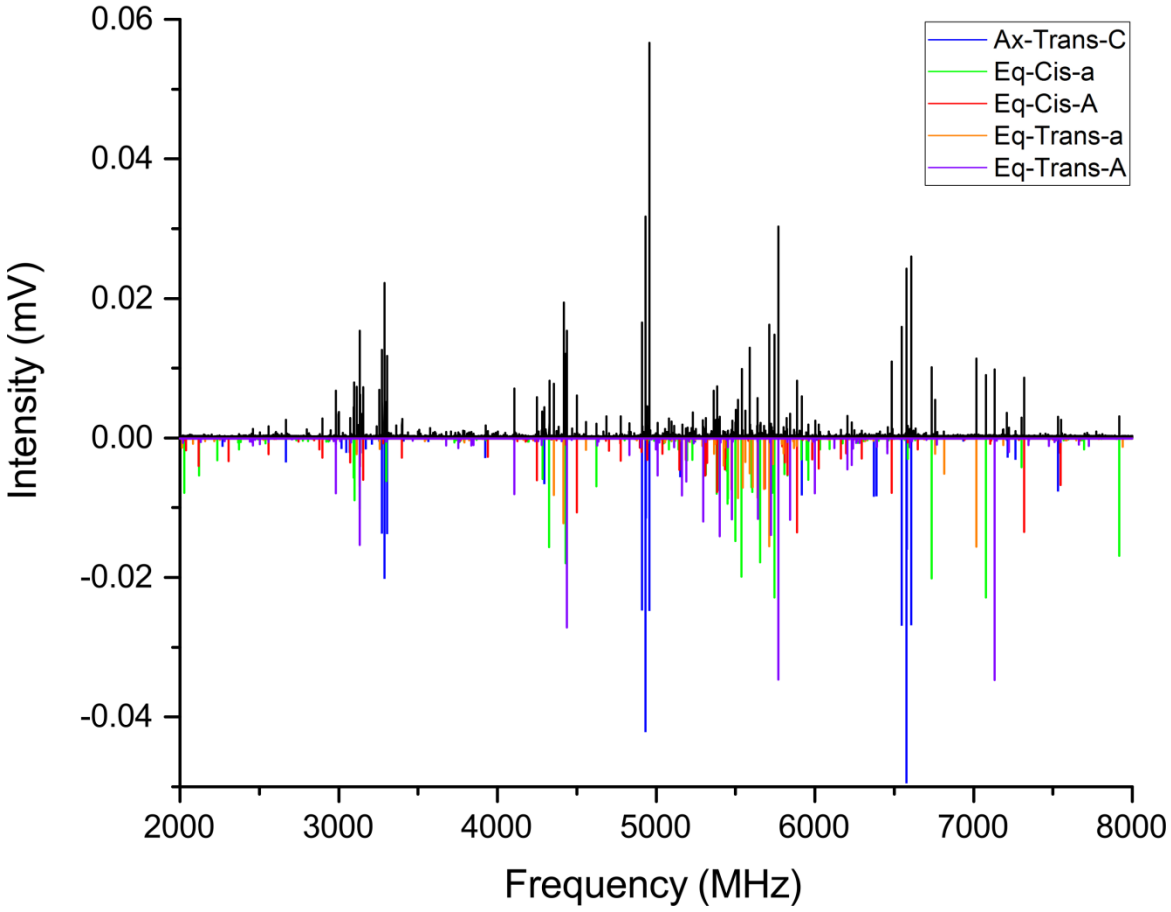
0.06
0.04
0.02
0.00
-0.02
-0.04
Intensity (mV)
2000
3000
4000
5000
6000
7000
8000
Frequency (MHz)
Ax-Trans-C
Eq-Cis-a
Eq-Cis-A
Eq-Trans-a
Eq-Trans-A

FIGURE 4

a)

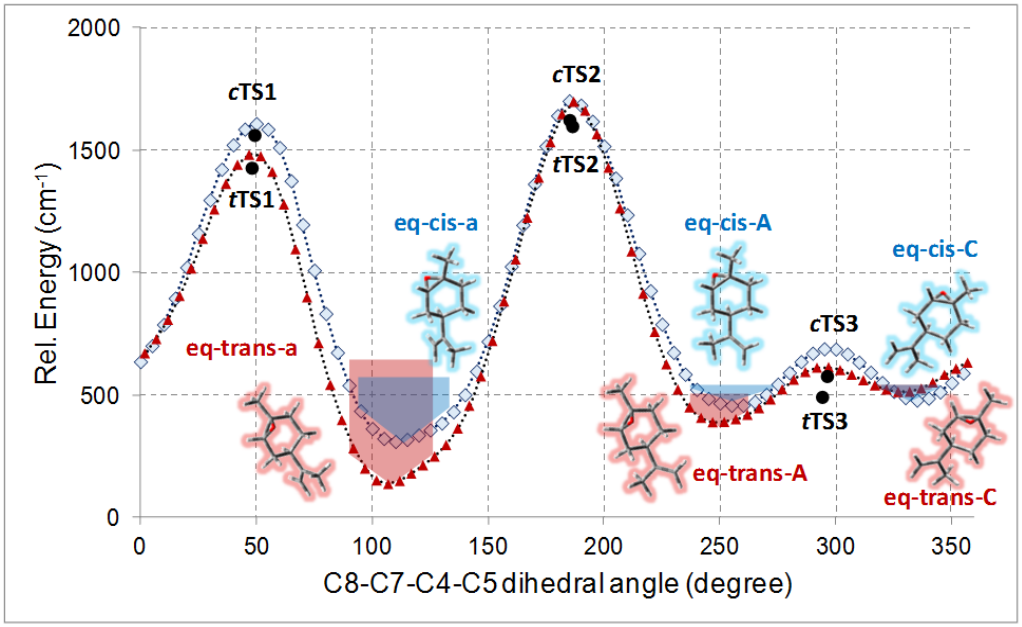
2000
1500
1000
500
0
Rel. Energy (cm-1)
cTS1
tTS1
cTS2
tTS2
cTS3
tTS3
eq-cis-a
eq-cis-A
eq-cis-C
eq-trans-a
eq-trans-A
eq-trans-C
0
50
100
150
200
250
300
350
C8-C7-C4-C5 dihedral angle (degree)

b)

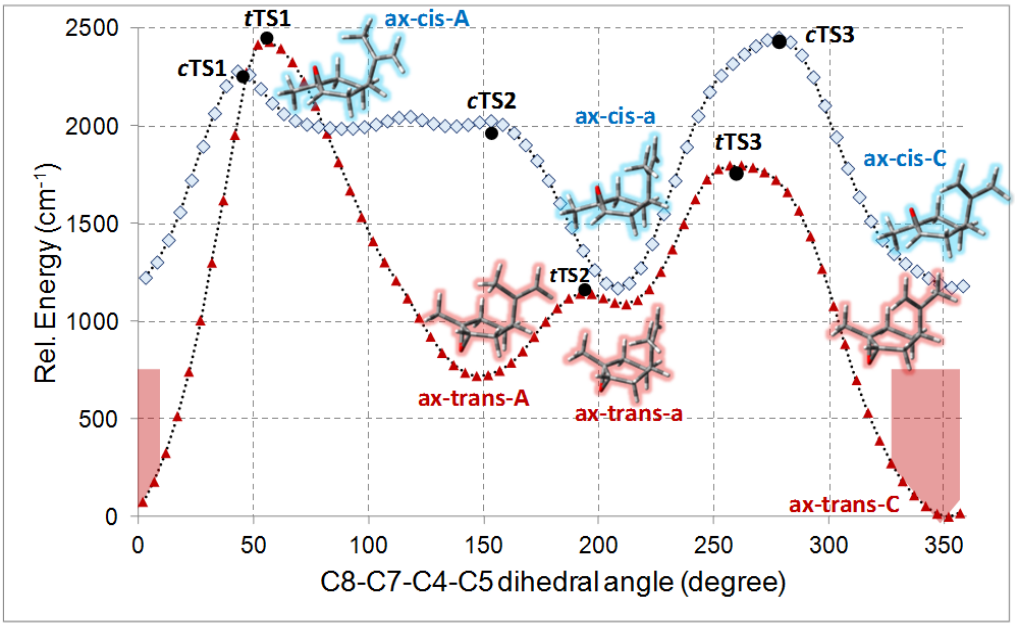
2500
2000
1500
1000
500
0
Rel. Energy (cm-1)
tTS1
cTS1
ax-cis-A
cTS2
ax-cis-a
cTS3
tTS3
ax-cis-C
tTS2
ax-trans-A
ax-trans-a
ax-trans-C
0
50
100
150
200
250
300
350
C8-C7-C4-C5 dihedral angle (degree)

TABLE 1. Relative energies of the twelve conformers of limonene oxide from several levels of theory.

Conformers	**Relative energy (cm^{-1})[a]**								
	B3LYP[1]	**B3LYP[2]**	**B3LYP[3]**	**M062X[1]**	**M062X[2]**	**MP2[1]**	**MP2[4]**	**G3**	**G4**
eq-trans-a	0	0	0	34	6	67	191	17	0
eq-trans-A	191	182	199	178	95	307	334	188	170
eq-cis-a	178	179	171	196	200	244	388	209	189
eq-cis-A	234	234	246	256	184	371	399	253	233
eq-cis-C	260	262	295	390	258	421	453	296	279
eq-trans-C	287	267	327	404	304	425	491	314	303
ax-trans-C	617	634	185	0	0	0	0	0	139
ax-trans-A	1295	1337	810	637	679	713	742	704	853
ax-cis-C	1425	1454	1114	1173	1096	1179	1258	1240	1281
ax-trans-a	1451	1457	1125	1103	1082	1145	1096	1037	1125
ax-cis-a	1681	1690	1275	1109	1110	1232	1178	1095	1111
ax-cis-A	1906	1966	1640	1927	1880	2014	2022	1873	1948

[a] All the relative energies are zero point corrected (ZPE, ΔE_0), except those calculated at the MP2/aug-cc-pVTZ level, which are equilibrium relative energies (ΔE_e). **[1]**: 6-311++G(d,p) basis set; **[2]**: 6-311++G(2df,p) basis set; **[3]:** B3LYP-D3/6-311G++(d,p); **[4]**: aug-cc-pVTZ basis set.

Table 2. Theoretical spectroscopic constants and dipole moment components of the axial and equatorial conformers of limonene oxide using MP2/6-311++G(d,p) including zero-point corrections.

Parameter	**eq-trans-a**	**eq-cis-a**	**eq-trans-A**	**eq-cis-A**	**eq-cis-C**	**eq-trans-C**	**ax-trans-C**	**ax-trans-A**	**ax-trans-a**	**ax-cis-C**	**ax-cis-a**	**ax-cis-A**
A[a] (MHz)	2488.0	2480.8	2476.2	2481.2	2485.7	2465.8	1822.3	1874.0	1689.2	1969.8	1813.0	2064.2
B (MHz)	643.4	652.5	654.8	671.5	657.6	662.8	852.7	853.7	876.9	840.1	907.2	787.4
C (MHz)	624.9	615.6	601.9	593.3	604.0	593.6	833.6	810.7	834.8	771.4	826.9	770.9
Δ (uÅ^2)	-179.9	-157.2	-136.2	-104.5	-135.1	-116.1	-263.8	-238.3	-270.1	-203.0	-224.7	-231.1
μ_a (D)	-0.2	-0.2	0.4	0.1	0.1	-0.5	-1.7	-1.1	-1.7	0.3	0.9	0.9
μ_b (D)	0.8	1.5	-0.4	-1.0	0.5	1.4	1.0	1.3	0.3	1.6	0.6	0.2
μ_c (D)	-1.4	1.6	-2.1	-1.3	-1.7	-1.7	-0.2	-0.2	-0.9	1.5	1.8	-2.0
$\Delta E_{MP2+ZPC}$(cm^{-1})	67	244	307	371	421	425	0	713	1145	1179	1232	2014
ΔG^{353} (cm^{-1})	0	167	173	213	359	280	77	768	1184	1266	1449	1911

[a] A, B, C are the rotational constants; Δ is the inertial defect, $\Delta = I_c - I_a - I_b$,where I_a, I_b and I_c are the moments of inertia along the principal axis of inertia; μ_a, μ_b, μ_c are the electric dipole moment components; ΔE and ΔG are the MP2/6-311++G(d,p) electronic energies including the zero-point correction, and Gibbs free energies (353 K), respectively (in cm^{-1}).

Table 3. Experimental spectroscopic constants of the five observed conformers of limonene oxide.

Parameter	**I** **eq-cis-a**	**II** **eq-trans-a**	**III** **eq-trans-A**	**IV** **eq-cis-A**	**V** **eq-trans-C**
A[a] (MHz)	2482.48326(37)[e]	2490.78133(54)	2479.21491(46)	2483.21481(71)	1852.7302(21)
B (MHz)	648.960264(65)	642.284591(90)	652.840122(61)	672.09401(25)	829.97836(79)
C (MHz)	614.849331(49)	621.891306(92)	599.644225(56)	588.38183(23)	814.50598(73)
D_J (kHz)	0.01897(21)	0.01410(33)	0.01432(28)	-	-
d_1 (kHz)	0.001450(92)	0.00104(16)	-	-	-
d_2 (kHz)	-	-	0.00157(44)	-	-
Δ (uÅ^2)	-160.37	-177.10	-135.17	-96.53	-261.21
a/*b*/*c*[b] (D)	vw/s/s	vw/m/s	w/w/s	no/m/m	s/m/no
σ[c] (kHz)	8.2	7.0	6.6	7.6	9.8
N[d]	74	58	65	31	21

[a] A, B and C are the rotational constants. D_J, d_1 and d_2 are the centrifugal distortion constants.
[b] *a*, *b* and *c* are the type of transitions observed (no: not observed, vw:very weak, w:weak, m:medium, s:strong)
[c] σ is the rms deviation of the fit.
[d] N is the number of the fitted transitions.
[e] Standard error in parentheses in units of the last digit.